Translational Oncology
www.transonc.com

Volume 2 Number 2 June 2009 pp. 89–95 89

Modeling Adult Gliomas Using RCAS/*t-va* Technology[1,2]

Dolores Hambardzumyan*,†,3, Nduka M. Amankulor*,†,‡,3, Karim Y. Helmy*,†, Oren J. Becher*,†,§ and Eric C. Holland*,†,¶,#

*Department of Cancer Biology and Genetics, Memorial Sloan-Kettering Cancer Center, New York, NY 10021, USA; †Brain Tumor Center, Memorial Sloan-Kettering Cancer Center, New York, NY 10021, USA; ‡Department of Neurosurgery, Yale University School of Medicine, New Haven, CT, USA; §Department of Pediatrics, Memorial Sloan-Kettering Cancer Center, New York, NY 10021, USA; ¶Department of Neurosurgery, Memorial Sloan-Kettering Cancer Center, New York, NY 10021, USA; #Department of Surgery, Memorial Sloan-Kettering Cancer Center, New York, NY 10021, USA

Abstract

Malignant gliomas remain the most devastating childhood and adult tumors of the central nervous system. Although adult and pediatric gliomas are histologically indistinguishable, they differ in location, behavior, and molecular characteristics. This implies that the molecular pathways and pathophysiology of malignant gliomagenesis in these two populations are distinct. Such differences between adult and pediatric gliomas may predict different therapeutic responses. Therefore, accurate genetically engineered models of adult and pediatric gliomas may help understand the biology of these tumors and evaluate therapeutic agents in preclinical studies. It has been proposed that gliomas arise from the subventricular zone in mice during development. Here, we demonstrate that, in adult mice, gliomas may arise not only when injected in the subventricular zone but also when injected in the cortex and cerebellum. Our work demonstrates a versatile and highly reproducible adult mouse model of glioma, which can be easily incorporated into preclinical studies.

Translational Oncology (2009) 2, 89–95

Introduction

Malignant gliomas constitute a genetically and histologically heterogeneous group of tumors associated with significant mortality and morbidity [1]. These tumors occur in children; however, they are far more prevalent in adults. In adults, high-grade gliomas are composed of anaplastic astrocytoma (AA), anaplastic oligodendroglioma, and glioblastoma multiforme (GBM). They can also exist as mixed lineage tumors, most commonly as anaplastic oligoastrocytoma [1]. In general, malignant gliomas progress rapidly and are resistant to therapy [2]. The survival rate for GBM is approximately 1 year [2,3], 2 years for AA, and 5 years for anaplastic oligodendroglioma [4]. Although the bulk of research in glioma biology relies on valuable tools such as passaged cell lines and xenograft models, there is growing evidence that these conditions do not represent a comprehensive scope of the cellular complexity human gliomas [5]. Brain tumors are diagnosed principally based on histologic characteristics, with less attention paid to the several known molecular alterations that occur commonly in gliomas, possibly contributing to the poor survival of GBM patients. Although the current histological diagnostic criteria provide good prognostic information, they do not inform optimum therapy. Illustrating this point, as standard of care, all patients with the diagnosis of high-grade gliomas are currently treated identically without consideration of the molecular variables that may impact treatment.

Address all correspondence to: Eric Holland or Dolores Hambardzumyan, 1275 York Ave, New York, NY 10021. E-mail: hollande@mskcc.org, hambardd@mskcc.org

[1]This work was supported by Brain Tumor Center. K.Y.H. is a Howard Hughes Medical Institute Medical Research Training Fellow.

[2]This article refers to supplementary materials, which are designated by Figures W1 and W2 and are available online at www.transonc.com.

[3]These authors contributed equally to this work.

Received 13 January 2009; Revised 13 January 2009; Accepted 14 January 2009

DOI 10.1593/tlo.09100

During the last two decades, a number of groups have sought to identify molecular subtypes of gliomas, an undertaking that remains a critical challenge for glioma biologists [2,6]. Genetic alterations found in adult gliomas have generally been divided into two groups. The first group contains genes that are related to growth factors, their receptors, and signal transduction pathways. These include anomalies of platelet-derived growth factor receptors (PDGFR1/2) [7–10], epidermal growth factor receptor [6,11,12], fibroblast growth factor receptor [13,14], ciliary neurotrophic factor [15], and hepatocyte growth factor/scatter factor [16]. The second group encompasses genes implicated in cell cycle regulation, such as the *INK4a-ARF* locus, which is altered in 60% of GBM [17], and the *RB* gene, which is altered in 33% of GBM [18]. Mutations in tumor suppressors *TP53* and *PTEN* are also common genetic alterations in human GBM [19]. In addition to the classification based on basic molecular alterations, GBM can be further subdivided into primary GBM, which arise *de novo*, and secondary glioblastomas that progress from lower-grade gliomas and likely constitute a highly heterogeneous group [2].

Our increased understanding of the diverse alterations in human gliomas and the potential significance of these alterations to therapeutic responses have increased the need for additional genetically engineered mouse models. Data obtained from preclinical evaluations of therapies using new genetically engineered mouse models that reflect the heterogeneity of human disease may open new treatment avenues. Furthermore, such studies may help to identify differences in response to therapeutic agents between the various subgroups of glioma and to facilitate the design of individualized therapeutic approaches based not only on histological characteristics but also on genetic alterations and tumor location.

To study glioma development, we have modeled gliomas using the RCAS/*tv-a* system to initiate tumors in newborn mice with known glioma oncogenic drivers. This model system allows somatic gene transfer of selected oncogenes, such as *PDGF* and *Kras*, into targeted brain cells engineered to express the tv-a receptor. These transgenic *tv-a* mice can then be crossed onto various genetic backgrounds to model the effects of genetic aberrations such as tumor suppressor loss on glioma formation and response to therapy. Using this model, we have observed that oncogenes such as *Kras* and *PDGF* produce gliomas with higher grade and shorter latency in mice with *Ink4a-Arf*–/– and *PTEN* loss backgrounds (mostly GBM) compared with wild type mice, which develop mostly low-grade tumors [20,21]. These studies provide important mechanistic insights into the role of specific tumor suppressor loss in *PDGF*- and *Kras*-induced pediatric gliomas. The short latency of high-grade glioma development in these tumor suppressor-loss backgrounds, results in animals injected while pups developing GBM when they are very small (~10-15 g). This feature of our pediatric RCAS/*tv-a* glioma model presents a challenge for use of these animals in long-term treatment experiments. Because of this limitation and the documented molecular differences between adult and pediatric gliomas [22–24], we sought to develop an adult glioma model using RCAS/*tv-a* methodology. The availability of valid adult glioma models that more easily permit preclinical therapeutic studies are urgently needed and, furthermore, will facilitate comparison of differences in the biology and therapeutic responses between adult and pediatric gliomas.

To generate gliomas in adult mice, we stereotactically delivered PDGFB into adult *tv-a* mice at various intracranial locations. We were able to generate gliomas by overexpressing oncogenes in nestin- and GFAP-positive cells of mice deleted for various tumor suppressors. These mice represent excellent tools for dissecting the role of location, genetic background, and cell of origin in the response to radiation and chemotherapy in adult gliomas. Data obtained from these studies can then be evaluated in parallel with data obtained from pediatric preclinical studies.

Using a stereotactic technique to infect cells in different regions of the brain in adult mice, we investigated the effect of location on the tumor initiating ability of a given oncogene. We chose the subventricular zones (SVZ), a region known to maintain central nervous system stem cells into adulthood, the left and right hemispheres, and the cerebellum. Our results demonstrate that PDGF-driven gliomagenesis is possible in the SVZ, cortex, and the cerebellum, suggesting that tumor-initiating cells responding to PDGF in adults may reside in different intracerebral locations.

Materials and Methods

Mice

Ntv-a wt, *Gtv-a wt*, *Gtv-a Ink4a–/–*, *Gtv-a Arf–/–*, *Gtv-a p53–/–*, *Ntv-a p53*, *Ntv-a Ink4a-Arf–/– LPTEN*, *Ntv-a Ink4a-Arf–/– Gli-luc*, *Gtv-a Ink4a-Arf–/– LPTEN* mice were used at an age range of 4 to 6 weeks for all experiments. The genetic backgrounds of *tv-a* mice are FVB/N, C57BL6, BALB/C, and 129. Generation of *tv-a*, *LPTEN*, and *Ink4a-Arf*, *p53* alleles has been described [25–28].

Cell Culture and Transfections

DF-1 cells were purchased from ATCC (Manassas, VA). Cells were grown at 39°C according to ATCC instructions. Transfections with RCAS-PDGFB-HA, and RCAS-CRE were performed using Fugene 6 transfection kit (no. 11814443001; Roche, Mannheim, Germany) according to manufacturer's protocol.

Intracranial Injections

Injections were performed using stereotactic fixation device (Stoelting, Wood Dale, IL). Mice used for these experiments were adult from 4 to 6.5 weeks old [29,30]. There was no significant difference in tumor latency or incidence in this age range (data not shown). Mice were anesthetized with intraperitoneal injections of ketamine (0.1 mg/g) and xylazine (0.02 mg/g). One microliter (for single injections or 1:1 mixture for combined injections) of 4×10^4 transfected DF-1 cell suspension was delivered using a 30-gauge needle attached to a Hamilton syringe. Locations were determined according to the instructions in the atlas [31]. Two sets of coordinates for SVZ and right hemosphere were used. Coordinates for SVZ injections were bregma 0 mm, Lat (lateral) –0.5 mm (right of midline), and a depth –1.5 mm from the dural surface; bregma 1.7 mm, Lat –0.5 mm, and a depth 2.5 mm. Left and right hemisphere: AP (Anteroposterior) –2 mm posterior to bregma, Lat –0.5 mm (left or right) depth –1 mm from dural surface; bregma 0.5 mm, Lat 2 mm, and a depth 1 mm. Cerebellum: AP –5.5 mm from bregma. Lat –1.5 mm (to the left), depth –1.5 mm from the dural surface. Mice were monitored carefully and sacrificed when they displayed symptoms of tumor development (lethargy, head tilt).

Tissue Processing

Animals used for histological analysis were killed, and brains were removed and fixed in 10% neutral-buffered formalin for 72 hours.

Fixed tissues were then embedded in paraffin. Formalin-fixed, paraffin-embedded specimens were serially sectioned and slide-mounted. The sections were deparaffinized in histoclear (Richard-Allan Scientific, Walldorf, Germany) and were passed through graded alcohols before staining with a hematoxylin and eosin (H&E) reagent.

Immunohistochemistry

An automated staining processing (Discovery; Ventana Medical Systems, Inc., Tucson, AZ) was used for immunohistochemical detection. The protocols were established at the Molecular Cytology Core Facility and at the Brain Tumor Center, Memorial Sloan-Kettering Cancer Center. Anti-PCNA antibodies were obtained from Dako (no. MO879; Glostrup, Denmark), anti-Ki67 from Vector (VP-RMO4, Burlingame, CA), and anti-pH3(Ser10) from Upstate (Lake Placid, NY) (06-570) and were used at 1:2000, 1:200, and 1:800 dilutions in 2% BSA in PBS correspondingly.

Bioluminescent Imaging

Mice were anesthetized with 3% isoflurane before retro-orbital injection with 75 mg/kg body weight of luciferin (Xenogen, Hopkinton, MA). One minute after injection of the luciferin, images were acquired for 4 minutes with the IVIS (Xenogen). A photographic image was taken onto which the pseudocolor image representing the spatial distribution of photon count is projected. We defined a circular region of interest between the ears and used it as a standard in all experiments. From this region, photon counts are compared between different mice.

Magnetic Resonance Imaging

All animals were imaged with a custom-made ID 32-mm quadrature birdcage body resonator (Stark Contrast MRI Research, Erlangen, Germany) while anesthetized using 1.5% isoflurane (Terrell, MINRAD, Inc, Bethlehem, PA). All images were acquired on a Bruker USR 4.7T scanner (Bruker Biospin MRI, Inc, Billerica, MA). The mouse head was imaged in the coronal orientation using a T2-weighted fast spin-echo rapid acquisition with relaxation enhancement sequence with repetition time = 3.5 seconds, echo time = 50 milliseconds, rapid acquisition with relaxation enhancement factor of 8, number of acquisitions = 24, field of view = 3 × 2 cm, slice thickness = 0.7 mm, with an in-plane resolution of 117 × 156 mm. Animal breathing was monitored using an animal physiological monitor system (SA Instruments, Stony Brook, NY) [32].

Statistical Analysis

Kaplan-Meier survival curves have been made using GraphPad Prism 4 (GraphPad Software, San Diego, CA) and analyzed using log-rank (Mantel-Cox) test: $^{*}P < .05$; $^{**}P < .01$; $^{***}P < .001$; and absence of star, not significant.

Results

*RCAS/*tv-a *System Allows Generation of Adult Gliomas When Injected in the SVZ*

The RCAS/tv-a model has been a very useful and productive tool for studying pediatric brain tumors [33–36]. During the last few years, data from genomic studies have revealed substantial molecular differences between pediatric and adult malignant gliomas. For example, loss of the *PTEN* gene and amplification epidermal growth factor receptor are uncommon in pediatric malignant gliomas, whereas these changes frequently occur in adults [22]. Differences in genetics can result in diverse responses to therapy in adult and pediatric gliomas. To model adult gliomas in mice, we delivered expression of the *PDGFB* gene into the SVZ, where nestin- and GFAP-positive progenitor cells reside in normal brain [37]. Mechanically, we stereotactically injected vector-infected chicken fibroblasts (DF-1) producing RCAS-PDGFB into the SVZ of adult mice from 4- to 6.5-week-old transgenic mice expressing the *tv-a* receptor on nestin-positive cells (*Ntv-a* mice). Survival results demonstrated that injection of RCAS-PDGFB alone into the SVZ of *Ntv-a* mice resulted in long latency to tumor formation, but when RCAS-PDGFB was introduced into *Ntv-a* mice with germ line *Ink4a-Arf* loss, tumor latency was decreased and tumor grade was significantly increased (Figure 1*A*). Approximately 16% of *Ntv-a* mice injected with RCAS-PDGFB into the SVZ developed tumors with low-grade histologic finding, whereas when RCAS-PDGF was injected into the SVZ of *Ntv-a Ink4a-Arf*−/− mice, tumor incidence was 100% and most tumors displayed microvascular proliferation and pseudopalisading necrosis, histologic characteristics of human GBM (Figure 1, *B* and *C*). Tumors generated when injected into the SVZ were mainly located adjacent to the lateral ventricles in the frontal lobe with extension into the olfactory bulb.

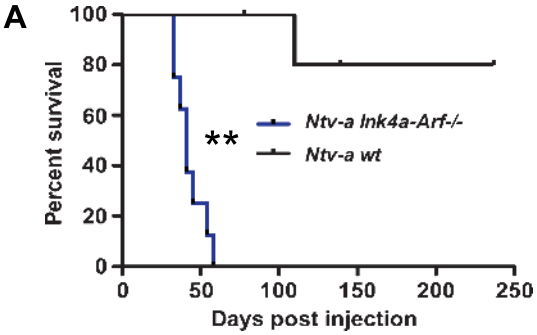

B

Number of mice injected PDGF in SVZ		Number of mice that developed tumor	% tumor formation
Ntv-a Ink4a-Arf-/-/	(8)	8	100
Ntv-a wt	(6)	1	16

C

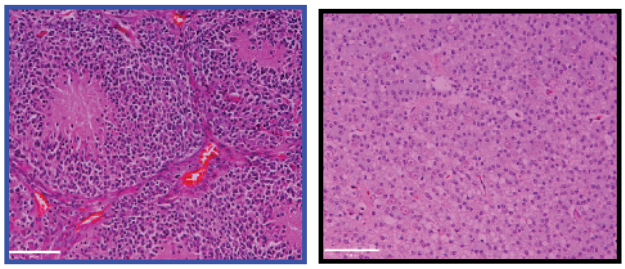

Figure 1. RCAS/*tv-a* system allows generation of adult gliomas in the frontal lobe, when *Ntv-a* cells are targeted cells in the SVZ by PDGFB. (A) Kaplan-Meier survival curve shows that PDGFB overexpression in the SVZ of *Ntv-a* wt mice induces low-grade gliomas with low incidence compared with *Ntv-a Ink4a-Arf*−/− background, which leads to GBM formation with shorter latency. All the mice without obvious evidence of tumors were killed 235 days after injection. (B) Table showing the tumor incidence (%) by PDGFB overexpression in *Ntv-a* and *Ntv-a Ink4a-Arf*−/− backgrounds. (C) Corresponding H&Es for A. Scale bar, 74 μm.

Generation of Gliomas in Different Locations

Recent studies from two different groups have suggested that histologically similar tumors located in different brain regions are molecularly distinct, raising the possibility that these tumors might arise from different cells of origin [38–40]. To model the tumorigenic potential of different locations in the mammalian brain, we injected RCAS-PDGFB DF-1 producer cells in combination with RCAS-Cre (to induce PTEN loss in mice harboring the floxed *PTEN* transgene) in four different locations in *Ntv-a Ink4a-arf−/− LPTEN mice*: 1) the SVZ, 2) the right and the 3) left cerebral hemispheres, and 4) the cerebellum. Figure 2*A* depicts the Kaplan-Meier survival curve of mice injected in these four different locations. Mice injected in either the SVZ or the right or left cerebral hemispheres show similar survival, whereas mice injected in the cerebellum exhibit significantly longer survival compared with the other three locations. In summary, all of the mice injected in the SVZ and the right and left cerebral hemispheres developed tumors, whereas 83% of cerebellum-injected mice developed tumors (Figure 2*B*). Tumors initiated in all four locations were histologically similar and demonstrated features of GBM (Figure 2*C*), including microvascular proliferation and extensive areas of pseudopalisading necrosis (Figure 2*C*). Platelet-derived growth factor receptor injection with/or without *PTEN* loss (Figures 2, *A* and *C*, and W1*A*) in the SVZ results in tumor formation in the SVZ with extension into the ipsilateral frontal lobe and olfactory bulb, suggesting that these tumors may migrate within the rostral migratory stream in agreement with published literature [30]. In contrast, tumors initiated at the right and left hemispheres produced tumors with diffuse cortical involvement with no extension into the olfactory bulb and no extension into the brainstem or cerebellum. In agreement with human data [41,42], tumor formation resulting from cerebellar injections occurred at lower frequency compared with the other locations. Nevertheless, high-grade tumors arose when PDGFB was injected within the cerebellum with or without *PTEN* loss (Figures 2*A* and W1, *A* and *B*). All tumors generated by these methods exhibited similar proliferation rates as determined by immunostaining for PCNA Ki67 and pH3, regardless of location (Figures 2*D* and W2).

Targeting PDGF to GFAP-Expressing SVZ Cells in Gtv-a *(GFAP-*tv-a*) Mice Leads to GBM Formation with Mixed Oligoastrocytoma Histology*

Most genetic alterations occurring in human gliomas result in signal transduction abnormalities or disruption of cell cycle control pathways [43]. The CDKN2A locus, which encodes $p16^{Ink4A}$ and $p14^{ARF}$, is deleted in approximately 60% of human GBM [18], and the incidence of

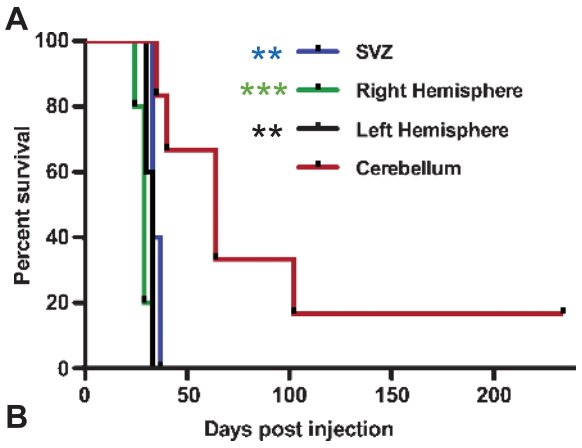

Number of injected mice and locations		Number of mice that developed tumor	% tumor formation
SVZ	(5)	5	100
Right H	(5)	5	100
Left H	(5)	5	100
Cerebellum	(6)	5	83

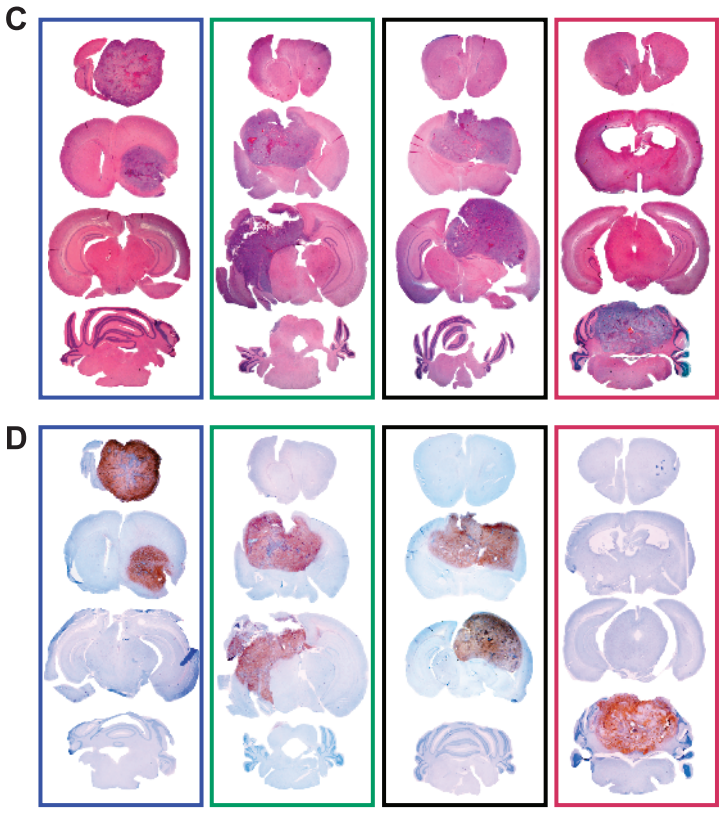

Figure 2. RCAS/*tv-a* system allows generation of tumors in different locations of adult *Ntv-a* mice overexpressing PDGFB in combination with *PTEN* loss. (A) Kaplan-Meier survival curve of mice injected with PDGF in combination with *PTEN* loss (through coinjection with Cre) in different locations of *Ntv-a Ink4a-Arf−/−LPTEN* mice demonstrated a tumorigenic advantage of the SVZ and the right and left hemispheres *versus* the cerebellum. (B) Table showing the number of mice injected and tumor incidence (%) by PDGFB overexpression in combination with *PTEN* loss in *Ntv-a Ink4a-Arf−/−lPTEN* background. (C and D) Whole-mount H&Es and PCNA immunostaining for the corresponding groups in Kaplan-Meier survival curve in the boxes corresponding to the color of each group. Statistical analysis was performed to compare all the groups to the cerebellar group. Statistical significance is represented by star (Figure 3*A*). Statistical analysis between right and left hemispheres and SVZ shows the slight advantage of the right hemisphere compared with SVZ (*). All the mice without obvious evidence of tumors were killed at 235 days after injection.

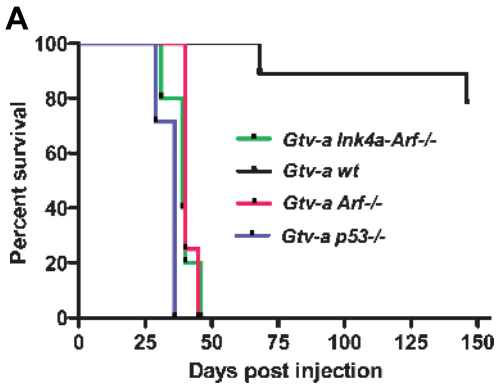

B

Number of mice injected PDGF in SVZ and genetic backgrounds		Number of mice that developed tumor	% tumor formation
Gtv-a wt	(9)	2 (low grade)	22
Gtv-a p53-/-	(7)	7 (GBM)	100
Gtv-a Arf-/-	(4)	4 (GBM)	100
Gtv-a Ink4a-Arf-/-	(5)	5 (GBM)	100

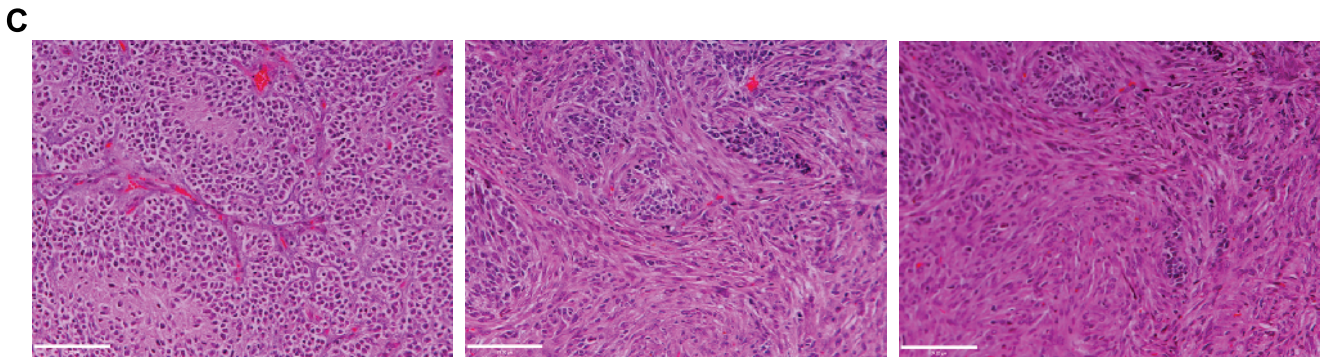

Figure 3. RCAS/*tv-a* system allows generation of tumors in different genetic backgrounds of adult *Gtv-a* mice by overexpressing PDGFB. (A) Kaplan-Meier survival curve of tumor-bearing mice injected with PDGF in the SVZ in different genetic backgrounds of *Gtv-a* mice. (B) Table showing the number of mice injected and tumor incidence (%) by PDGFB overexpression in different genetic backgrounds of *Gtv-a* mice. p53, Arf, or Ink4a-Arf loss cooperate with overexpression of PDGFB to induce high-grade gliomas. In contrast, PDGFB injection in *Gtv-a* wt mice leads to low-grade glioma formation with low incidence. (C) H&E micrographs showing tumors generated in *Gtv-a p53*−/− or *Arf*−/− or *Ink4a-Arf*−/− resemble mixed oligoastrocytoma histologic diagnosis. Scale bars, 74 μm. Statistical analysis reveals *** when Gtv-a/Ink4a-Arf−/−, Gtv-a/p53−/−, and Gtv-a/Arf−/− are compared with Gtv-a wt; Gtv-a/Ink4a-Arf−/− *versus* Gtv-a/Arf−/− is not significant; Gtv-a/p53−/− *versus* to Gtv-a/Arf−/− is **; Gtv-a/Ink4a-Arf−/− *versus* Gtv-a/p53−/− is *. All mice without obvious evidence of tumors were killed at 146 days after injection.

p53 mutations is 31% in GBM and 48% in AA [44]. We used *Gtv-a* transgenic mice (where the *tv-a* receptor is expressed on GFAP-positive cells) in *wt*, *p53*−/−, *Arf*−/−, and *Ink4a-Arf*−/− backgrounds to model the effect of cell cycle abnormalities in gliomas growing in different locations. As shown in Figure 3*A*, mice with tumors that were generated in backgrounds with deletions of *p53*, *Arf*, or *Ink4a-Arf* had significantly shorter latency compared with *wt*. Approximately 100% of mice injected in *Gtv-a p53*−/−, *Gtv-a Ink4a-Arf*−/−, and *Gtv-a Arf*−/− background develop GBM with oligoastrocytoma histologic finding, whereas only 22% of *Gtv-a* mice in a wild type background develop gliomas, all of which were low grade (Figure 3*B*). Tumors in *Gtv-a p53*−/−, *Gtv-a Ink4a-Arf*−/−, and *Gtv-a Arf*−/− background are GBM, composed of regions of more oligoastrocytoma and mixed astrocytoma histologies (Figure 3*C*).

Imaging of Tumor Bearing Mice with Gli-luc Bioluminescence and Magnetic Resonance Imaging

We recently reported the generation of a Gli-luc reporter mouse that can be used to noninvasively image Gli activity *in vivo*. We demonstrated that Gli activity, measured by luciferase bioluminescence (BLI), correlates with tumor grade [45]. To investigate whether Gli activity can also be used to image adult PDGF-induced gliomas, we injected RCAS-PDGFB through the stereotactic technique into the SVZ of *Ntv-a Ink4aArf*−/− Gli-luc adult mice. Similar to pediatric tumors modeled with the RCAS/*tv-a* system, we noted increased bioluminescence at the tumor site in stereotactically injected adult mice. Figure 4, *A* and *B*, shows an example of a BLI image of non–tumor- and tumor-bearing mice correspondingly; these tumors can also be imaged *ex vivo* as shown in the *top right panel* of Figure 4*B*. BLI imaging of these mice is a useful tool to monitor tumor response to therapy *in vivo*. To demonstrate shared characteristics between RCAS/*tv-a*–generated tumors in adult mice and their human counterparts, we imaged our tumor-bearing mice using magnetic resonance imaging (MRI). Notably, these tumors share many imaging characteristics with human GBM, as depicted by T2-weighted images of normal mouse brain (Figure 4*C*) and a tumor-bearing mouse stereotactically injected in the SVZ (Figure 4*D*). In summary, both MRI and BLI can be used to monitor tumor presence and response to therapy *in vivo* in preclinical trials.

Discussion

Mouse models of gliomas have been instrumental for investigating the causative factors for this heterogeneous disease. Furthermore, reliable and accurate models are essential in the implementation of preclinical studies to identify and validate new therapeutic strategies. During the last decade, we have used the RCAS/*tv-a* technology for modeling pediatric brain tumors, including pediatric gliomas. However, these models have limitations, most notably that the small

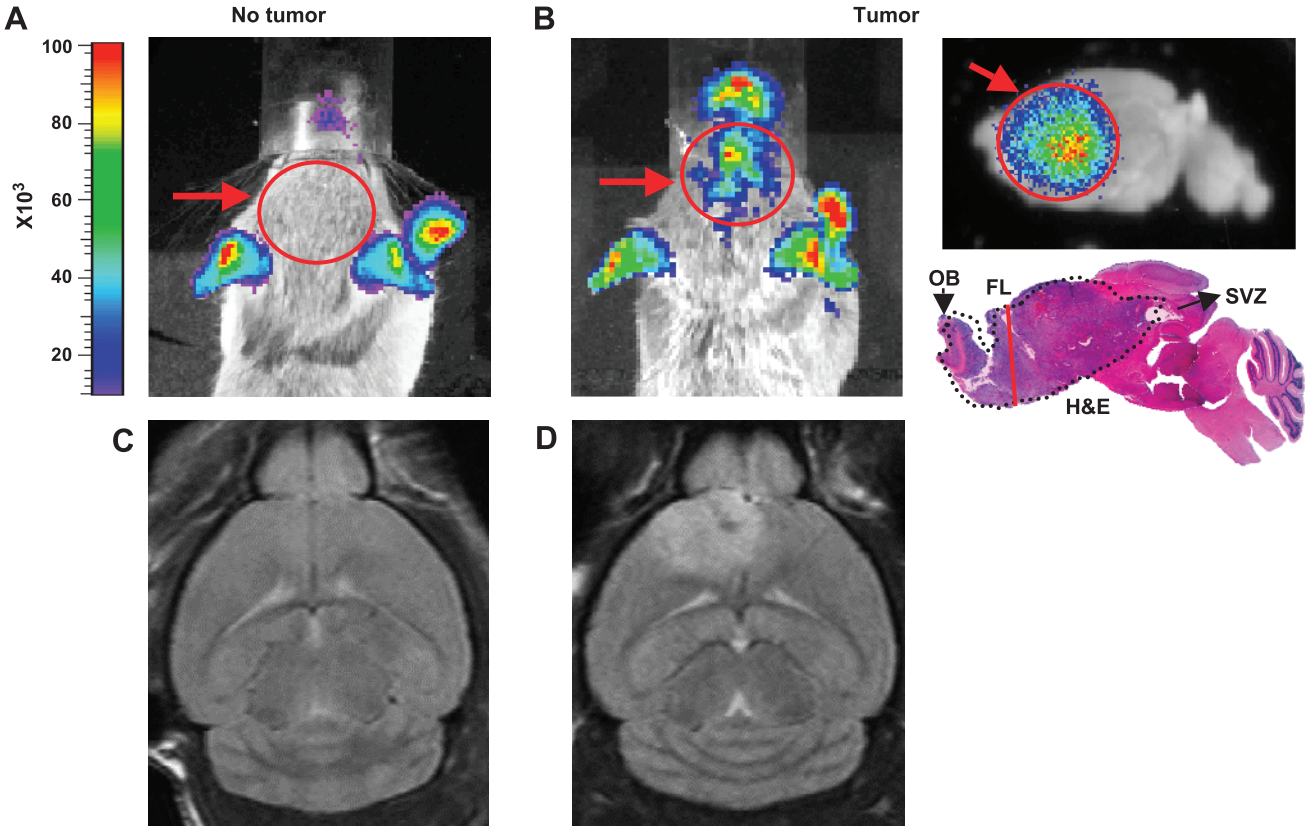

Figure 4. BLI and MRI are useful tools for visualization of tumors *in vivo*. (A) BLI image of non–tumor-bearing Gli-Luc mouse (red arrow and circle points to the brain, where there is no signal). (B) *In vivo* BLI image of PDGF-induced glioma injected in the SVZ, with *ex vivo* sagittal image of the same tumor with corresponding H&E. *FL* indicates frontal lobe; *OB*, olfactory bulb. (C and D) T2-weighted images of non–tumor- and tumor-bearing mice (injected with PDGF in the SVZ), respectively.

size of the mice at the time of tumor development poses significant difficulties when performing treatment studies that require long-term survival of the mice. In addition, several recent observations have indicated that childhood malignant gliomas have important biological characteristics that distinguish them from adult malignant gliomas [22–24]. These factors led us to develop a novel RCAS/*tv-a*–based model of adult gliomagenesis that could be used in parallel with our preexisting pediatric models. The existence of these two models now allows investigators to simultaneously compare the therapeutic responses of pediatric and adult gliomas in future studies.

Our study also attempts to lend insight into the influence of location on tumorigenic potential and tumor progression in an adult mammalian system of gliomagenesis (Figure W2). It is known that anatomic location in human gliomas influences prognosis and treatment options [46,47]. We demonstrated that RCAS-PDGFB injected into SVZ induced glioma formation in the SVZ and frontal lobe with extension into the olfactory bulb, a very common location for human gliomas [48]. We demonstrated that tumor incidence, latency, and mortality do not differ when tumors are generated in different locations in the cerebral hemispheres, including the SVZ. By contrast, tumors produced by cerebellar PDGFB overexpression are localized to the cerebellum with extension into the brainstem and occurred with lower incidence and with longer latency compared with cerebral hemisphere and SVZ injections.

Targeting nestin-positive or GFAP-positive cells when injected in the SVZ resulted in tumor formation with similar incidence and latency. We further demonstrated that loss of tumor suppressors *p53*, *Arf*, or *Ink4a-Arf* resulted in higher-grade tumors with shorter latency and 100% incidence compared with their wild type counterparts, in which only 22% of mice developed tumors, all of which are low grade. Finally, because the location of injection resulted in characteristic tumor locations in the mice, it is possible that a correlation exists between tumors and their cells of origin in humans as well.

Adult mice bearing tumors generated by stereotactic injections usually develop tumors when their weight range is 22 to 28 g, an ideal weight for treating mice, making these mice excellent tools for preclinical trials. BLI and MRI techniques further complement this technique, allowing noninvasive monitoring of therapeutic responses. This model will allow investigators to interrogate the role of tumor location, genetic background, and cell of origin (depending which cell type we target originally, nestin– or GFAP–) in response to therapy. We hope that data obtained from preclinical studies in these mouse models will contribute to the development of individual targeted therapies and accelerate the introduction of these therapies into human clinical trials for gliomas.

Acknowledgments

The authors thank Jim Finney and Quanchao Zhang for technical assistance. Technical assistance by Lupu and Winkleman from the Memorial Sloan-Kettering Cancer Center animal imaging core is appreciated.

References

[1] Prados MD and Levin V (2000). Biology and treatment of malignant glioma. *Semin Oncol* **27**, 1–10.

[2] Shai R, Shi T, Kremen TJ, Horvath S, Liau LM, Cloughesy TF, Mischel PS, and Nelson SF (2003). Gene expression profiling identifies molecular subtypes of gliomas. *Oncogene* **22**, 4918–4923.

[3] Stupp R, Mason WP, van den Bent MJ, Weller M, Fisher B, Taphoorn MJ, Belanger K, Brandes AA, Marosi C, Bogdahn U, et al. (2005). Radiotherapy plus concomitant and adjuvant temozolomide for glioblastoma. *N Engl J Med* **352**, 987–996.

[4] Winger MJ, Macdonald DR, Schold SC Jr, and Cairncross JG (1989). Selection bias in clinical trials of anaplastic glioma. *Ann Neurol* **26**, 531–534.

[5] Lee J, Kotliarova S, Kotliarov Y, Li A, Su Q, Donin NM, Pastorino S, Purow BW, Christopher N, Zhang W, et al. (2006). Tumor stem cells derived from glioblastomas cultured in bFGF and EGF more closely mirror the phenotype and genotype of primary tumors than do serum-cultured cell lines. *Cancer Cell* **9**, 391–403.

[6] Mischel PS, Shai R, Shi T, Horvath S, Lu KV, Choe G, Seligson D, Kremen TJ, Palotie A, Liau LM, et al. (2003). Identification of molecular subtypes of glioblastoma by gene expression profiling. *Oncogene* **22**, 2361–2373.

[7] Nister M, Libermann TA, Betsholtz C, Pettersson M, Claesson-Welsh L, Heldin CH, Schlessinger J, and Westermark B (1988). Expression of messenger RNAs for platelet-derived growth factor and transforming growth factor-alpha and their receptors in human malignant glioma cell lines. *Cancer Res* **48**, 3910–3918.

[8] Shih AH and Holland EC (2006). Platelet-derived growth factor (PDGF) and glial tumorigenesis. *Cancer Lett* **232**, 139–147.

[9] Hermanson M, Funa K, Hartman M, Claesson-Welsh L, Heldin CH, Westermark B, and Nister M (1992). Platelet-derived growth factor and its receptors in human glioma tissue: expression of messenger RNA and protein suggests the presence of autocrine and paracrine loops. *Cancer Res* **52**, 3213–3219.

[10] Di Rocco F, Carroll RS, Zhang J, and Black PM (1998). Platelet-derived growth factor and its receptor expression in human oligodendrogliomas. *Neurosurgery* **42**, 341–346.

[11] Libermann TA, Nusbaum HR, Razon N, Kris R, Lax I, Soreq H, Whittle N, Waterfield MD, Ullrich A, and Schlessinger J (1985). Amplification, enhanced expression and possible rearrangement of EGF receptor gene in primary human brain tumours of glial origin. *Nature* **313**, 144–147.

[12] Ekstrand AJ, James CD, Cavenee WK, Seliger B, Pettersson RF, and Collins VP (1991). Genes for epidermal growth factor receptor, transforming growth factor alpha, and epidermal growth factor and their expression in human gliomas *in vivo*. *Cancer Res* **51**, 2164–2172.

[13] Morrison RS, Yamaguchi F, Bruner JM, Tang M, McKeehan W, and Berger MS (1994). Fibroblast growth factor receptor gene expression and immunoreactivity are elevated in human glioblastoma multiforme. *Cancer Res* **54**, 2794–2799.

[14] Yamaguchi F, Saya H, Bruner JM, and Morrison RS (1994). Differential expression of two fibroblast growth factor-receptor genes is associated with malignant progression in human astrocytomas. *Proc Natl Acad Sci USA* **91**, 484–488.

[15] Weis J, Schonrock LM, Zuchner SL, Lie DC, Sure U, Schul C, Stogbauer F, Ringelstein EB, and Halfter H (1999). CNTF and its receptor subunits in human gliomas. *J Neurooncol* **44**, 243–253.

[16] Abounader R and Laterra J (2005). Scatter factor/hepatocyte growth factor in brain tumor growth and angiogenesis. *Neuro Oncol* **7**, 436–451.

[17] Schmidt EE, Ichimura K, Reifenberger G, and Collins VP (1994). *CDKN2* (p16/MTS1) gene deletion or CDK4 amplification occurs in the majority of glioblastomas. *Cancer Res* **54**, 6321–6324.

[18] Ueki K, Ono Y, Henson JW, Efird JT, von Deimling A, and Louis DN (1996). *CDKN2/p16* or *RB* alterations occur in the majority of glioblastomas and are inversely correlated. *Cancer Res* **56**, 150–153.

[19] Hill C, Hunter SB, and Brat DJ (2003). Genetic markers in glioblastoma: prognostic significance and future therapeutic implications. *Adv Anat Pathol* **10**, 212–217.

[20] Becher OJ and Holland EC (2006). Genetically engineered models have advantages over xenografts for preclinical studies. *Cancer Res* **66**, 3355–3358; discussion 3358–3359.

[21] Fomchenko EI and Holland EC (2006). Mouse models of brain tumors and their applications in preclinical trials. *Clin Cancer Res* **12**, 5288–5297.

[22] Pollack IF, Hamilton RL, James CD, Finkelstein SD, Burnham J, Yates AJ, Holmes EJ, Zhou T, and Finlay JL (2006). Rarity of PTEN deletions and EGFR amplification in malignant gliomas of childhood: results from the Children's Cancer Group 945 cohort. *J Neurosurg* **105**, 418–424.

[23] Rood BR and MacDonald TJ (2005). Pediatric high-grade glioma: molecular genetic clues for innovative therapeutic approaches. *J Neurooncol* **75**, 267–272.

[24] Warren KE (2008). Pediatric high-grade gliomas. *ASCO Educational Book*, 472–477.

[25] Trotman LC, Niki M, Dotan ZA, Koutcher JA, Di Cristofano A, Xiao A, Khoo AS, Roy-Burman P, Greenberg NM, Van Dyke T, et al. (2003). Pten dose dictates cancer progression in the prostate. *PLoS Biol* **1**, E59.

[26] Schaper J and van de Heyning J (1976). Cholesteatoma of the middle ear in human patients. An ultrastructural study. *Arch Otolaryngol* **102**, 663–668.

[27] Hu X, Pandolfi PP, Li Y, Koutcher JA, Rosenblum M, and Holland EC (2005). mTOR promotes survival and astrocytic characteristics induced by Pten/AKT signaling in glioblastoma. *Neoplasia* **7**, 356–368.

[28] Dai C, Celestino JC, Okada Y, Louis DN, Fuller GN, and Holland EC (2001). PDGF autocrine stimulation dedifferentiates cultured astrocytes and induces oligodendrogliomas and oligoastrocytomas from neural progenitors and astrocytes *in vivo*. *Genes Dev* **15**, 1913–1925.

[29] Fox JG, Anderson LC, Loew FM, and Quimby FW (2002). *Laboratory Animal Medicine.* San Diego, CA: Academic Press; 43 – Table VII.

[30] Alcantara Llaguno S, Chen J, Kwon CH, Jackson EL, Li Y, Burns DK, Alvarez-Buylla A, and Parada LF (2009). Malignant astrocytomas originate from neural stem/progenitor cells in a somatic tumor suppressor mouse model. *Cancer Cell* **15**, 45–56.

[31] Keith BJ and Franklin GP (1997). *The Mouse Brain in Stereotaxic Coordinates* San Diego, CA: Academic Press.

[32] Koutcher JA, Hu X, Xu S, Gade TP, Leeds N, Zhou XJ, Zagzag D, and Holland EC (2002). MRI of mouse models for gliomas shows similarities to humans and can be used to identify mice for preclinical trials. *Neoplasia* **4**, 480–485.

[33] Uhrbom L and Holland EC (2001). Modeling gliomagenesis with somatic cell gene transfer using retroviral vectors. *J Neurooncol* **53**, 297–305.

[34] Begemann M, Fuller GN, and Holland EC (2002). Genetic modeling of glioma formation in mice. *Brain Pathol* **12**, 117–132.

[35] Uhrbom L, Dai C, Celestino JC, Rosenblum MK, Fuller GN, and Holland EC (2002). Ink4a-Arf loss cooperates with KRas activation in astrocytes and neural progenitors to generate glioblastomas of various morphologies depending on activated Akt. *Cancer Res* **62**, 5551–5558.

[36] Hesselager G and Holland EC (2003). Using mice to decipher the molecular genetics of brain tumors. *Neurosurgery* **53**, 685–694; discussion 695.

[37] Alvarez-Buylla A, Seri B, and Doetsch F (2002). Identification of neural stem cells in the adult vertebrate brain. *Brain Res Bull* **57**, 751–758.

[38] Sharma MK, Mansur DB, Reifenberger G, Perry A, Leonard JR, Aldape KD, Albin MG, Emnett RJ, Loeser S, Watson MA, et al. (2007). Distinct genetic signatures among pilocytic astrocytomas relate to their brain region origin. *Cancer Res* **67**, 890–900.

[39] Gilbertson RJ and Gutmann DH (2007). Tumorigenesis in the brain: location, location, location. *Cancer Res* **67**, 5579–5582.

[40] Taylor MD, Poppleton H, Fuller C, Su X, Liu Y, Jensen P, Magdaleno S, Dalton J, Calabrese C, Board J, et al. (2005). Radial glia cells are candidate stem cells of ependymoma. *Cancer Cell* **8**, 323–335.

[41] Guillamo JS, Monjour A, Taillandier L, Devaux B, Varlet P, Haie-Meder C, Defer GL, Maison P, Mazeron JJ, Cornu P, et al. (2001). Brainstem gliomas in adults: prognostic factors and classification. *Brain* **124**, 2528–2539.

[42] Demir MK, Hakan T, Akinci O, and Berkman Z (2005). Primary cerebellar glioblastoma multiforme. *Diagn Interv Radiol* **11**, 83–86.

[43] Holland EC (2001). Gliomagenesis: genetic alterations and mouse models. *Nat Rev Genet* **2**, 120–129.

[44] Shiraishi S, Tada K, Nakamura H, Makino K, Kochi M, Saya H, Kuratsu J, and Ushio Y (2002). Influence of p53 mutations on prognosis of patients with glioblastoma. *Cancer* **95**, 249–257.

[45] Becher OJ, Hambardzumyan D, Fomchenko EI, Momota H, Mainwaring L, Bleau AM, Katz AM, Edgar M, Kenney AM, Cordon-Cardo C, et al. (2008). Gli activity correlates with tumor grade in platelet-derived growth factor–induced gliomas. *Cancer Res* **68**, 2241–2249.

[46] Simpson JR, Horton J, Scott C, Curran WJ, Rubin P, Fischbach J, Isaacson S, Rotman M, Asbell SO, Nelson JS, et al. (1993). Influence of location and extent of surgical resection on survival of patients with glioblastoma multiforme: results of three consecutive Radiation Therapy Oncology Group (RTOG) clinical trials. *Int J Radiat Oncol Biol Phys* **26**, 239–244.

[47] Jeremic B, Grujicic D, Antunovic V, Djuric L, Stojanovic M, and Shibamoto Y (1994). Influence of extent of surgery and tumor location on treatment outcome of patients with glioblastoma multiforme treated with combined modality approach. *J Neurooncol* **21**, 177–185.

[48] Larjavaara S, Mantyla R, Salminen T, Haapasalo H, Raitanen J, Jaaskelainen J, and Auvinen A (2007). Incidence of gliomas by anatomic location. *Neuro Oncol* **9**, 319–325.

A

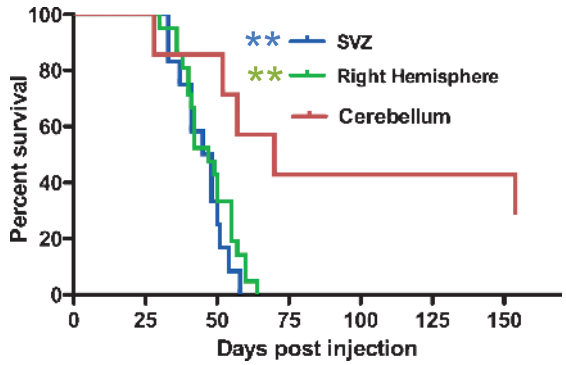

B

Number of injected mice and locations		Number of mice that developed tumor	% tumor formation
SVZ	(12)	12	100
Right H	(21)	21	100
Cerebellum	(7)	5	71.4

Figure W1. RCAS/*tv-a* system allows generation of tumors in different locations of adult *Ntv-a* mice by overexpressing PDGFB. (A) Kaplan-Meier survival curve of mice injected with PDGF in different locations of *Ntv-a Ink4a-Arf*−/− mice demonstrated a tumorigenic advantage of the SVZ and the right hemisphere *versus* the cerebellum. Statistical analysis was performed to compare all the groups to the cerebellar group. Statistical significance is represented by star. Statistical analysis shows significant advantage of the right hemisphere and SVZ compared with the cerebellum (**). (B) Table showing the number of mice injected and tumor incidence (%) by PDGFB overexpression in *Ntv-a Ink4a-Arf*−/− background.

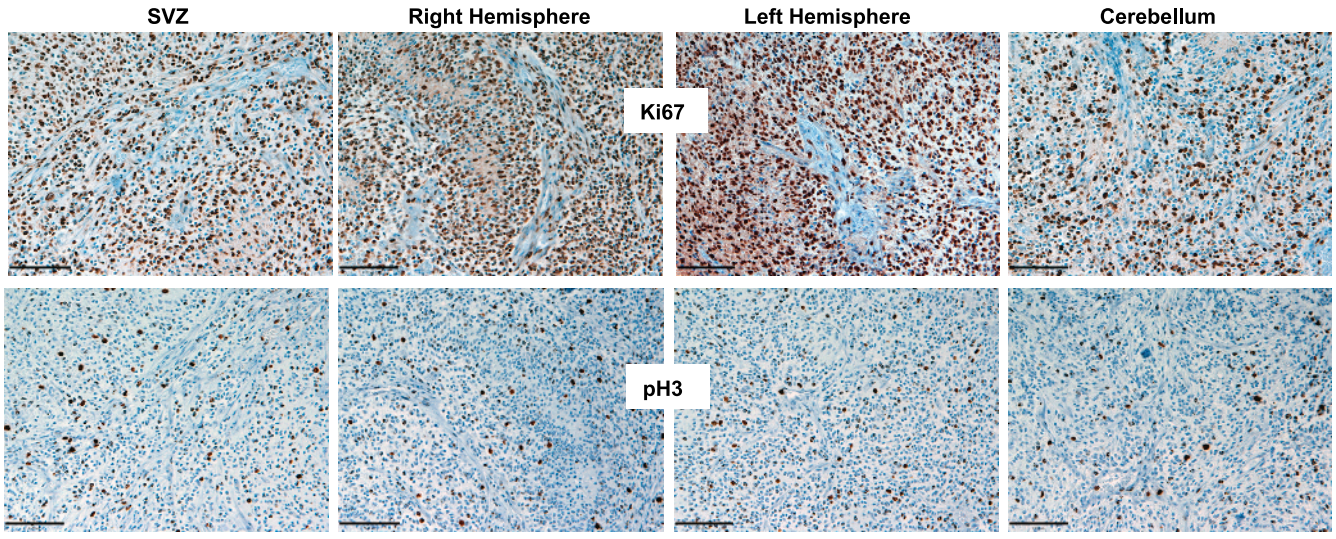

Figure W2. Tumors generated in different locations of adult *Ntv-a* mice overexpressing PDGFB in combination with *PTEN* loss show similar proliferative ability. Representative images of immunostaining for Ki67 and pH3 (Ser10) show similar level of positive cells in tumors generated by injecting PDGF in different locations of the brain. Scale bars, 74 μm.